JTTEE5 18:875–886
DOI: 10.1007/s11666-009-9354-x
1059-9630/$19.00 © ASM International

From DC Time-Dependent Thermal Plasma Generation to Suspension Plasma-Spraying Interactions

Erick Meillot, S. Vincent, C. Caruyer, J.P. Caltagirone, and D. Damiani

(Submitted January 30, 2009; in revised form May 4, 2009)

This paper proposes an original route for modeling the time-dependent behavior of a plasma jet issued from a DC plasma-spraying torch operating with various kinds of gas mixtures. The hydrodynamic interactions between this jet and a liquid jet for suspension plasma-spraying or a classical particle injection for the deposition of coatings are studied. In a first step, the classical plasma spraying process was explored using the FLUENT CFD code. Zirconia particles, defined as Lagrangian particles, were injected in an Ar/H_2 flow and their positions, kinetic and thermal states were compared with experimental results. The trend and intensity of the values demonstrated a rather good agreement. In a second step, the suspension plasma spraying was investigated with the AQUILON CFD to simulate interactions between the plasma and aqueous jets. An Ar/H_2 plasma flow was simulated with the Large Eddy Scale turbulence model assumption, in which a liquid jet had been introduced. The behavior observed during the first stage of the interactions between the two fluids corresponded to expectations.

Keywords 3D simulation, modeling, plasma jet, suspension, thermal plasma spraying, transient

1. Introduction

Nanomaterials are being employed in more and more fields due to their specific properties. For industrial applications requiring significant efficiency rates, thermal spraying can be one way to deposit coatings of varying width. Several surface treatment techniques can be employed, among which atmospheric plasma spraying (APS) involves a plasma gun as a thermal source transferring the electrical energy to input gas by Joule effect. This results in a high temperature and high velocity gas flow in which powder particles or suspensions are introduced. During the interaction with the gas jet, and after the evaporation of the media, the particles are subsequently fused and accelerated toward the material to be coated, thereby contributing to building up the coating by a piling of lamellae. For thick coatings, classical plasma or flame spraying processes can be used, whereas for thinner coatings, nanopowders are prepared in suspension and injected in a thermal source constituted of, for instance, a plasma jet or a flame.

Due to the plasma jet being relatively difficult to analyze (high temperature, high radiation) and because of the complex behavior of the process (the main parameters all being connected), simulation has a high potential as a numerical experimentation tool for obtaining an improved understanding of the interaction mechanisms.

The present paper investigates the possibility of simulating classical and suspension plasma spraying processes, and thus presents the actual global Thermal Spray Lab knowledge in modeling. The first step consists in obtaining the flow in which the materials are introduced. After a short review of the literature, the paper deals with the following sections:

- Plasma formation and the interaction of the jet with its environment,
- Classical plasma-spraying with injection of zirconia particles, and
- Suspension plasma-spraying.

The first section describes the progress in modeling concerning the phenomena of these three fields, after which recent developments and assumptions are presented. The third part presents simulated data from experiments, and the final section compares the results of these calculations with experimental data.

2. Progress in Plasma Jet

2.1 Plasma Generation

A classical plasma gun is exposed in Fig. 1 (Ref 1). Around a cylindrical cathode, generally in tungsten with thorium (2 wt.%), the operating gas (either pure, e.g., argon, or, more commonly, a mixture, e.g., argon/hydrogen, argon/hydrogen/helium) enters the torch and is

Erick Meillot, C. Caruyer, and **D. Damiani**, CEA-DAM, Le RIPAULT, F-37 260 Monts, France; and **S. Vincent** and **J.P. Caltagirone**, E.N.S.C.P.B., TREFLE Laboratory, F-33 607 Pessac, France. Contact e-mail: erick.meillot@cea.fr.

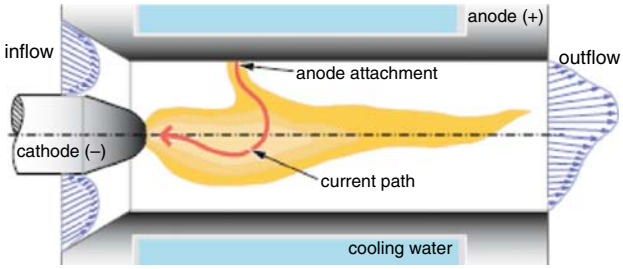

Fig. 1 A schematic of a DC plasma torch (Ref 1)

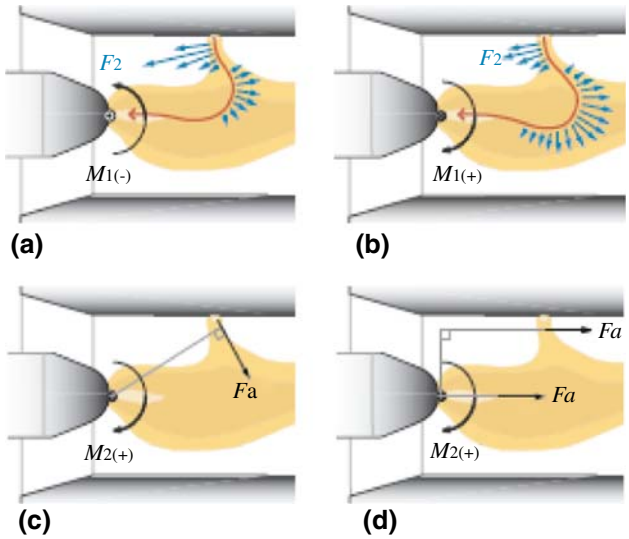

Fig. 2 A schematic of the electrical arc displacement in a DC plasma torch (Ref 1)

heated by the electrical arc generated between a nozzle-shaped anode (of oxygen-free copper) and the cathode. This results in the transformation of the gas into plasma, which exits the torch as a free jet. Despite the axis-symmetry of the geometry and the boundary conditions (i.e., the inflow velocity profile, constant anode potential), the flow behavior inside the torch is inherently three-dimensional due to the motion of the arc (i.e., the anode attachment) and therefore the plasma plume spreads outside the nozzle. The dynamic of the arc arises from the balance between the hydrodynamic (drag force and swirl or direct injection) and electromagnetic (Lorentz) forces applied to the incoming gas flow, both of which give rise to upstream, downstream and rotation displacements of the electrical attachment point (Fig. 2) (Ref 1).

This is amplified by the surface state of the nozzle (presence of asperities due to erosion, for instance) and the nature of the plasma gas leading to a thinner or thicker cold boundary layer (Ref 2, 3). The length of the arc is directly proportional to the variation of the arc voltage magnitude. As can be seen in Fig. 3, three main modes of torch running have been identified according to the arc voltage fluctuations (Ref 4) before the observation of an intermediate mode, thus mixing the characteristics of the

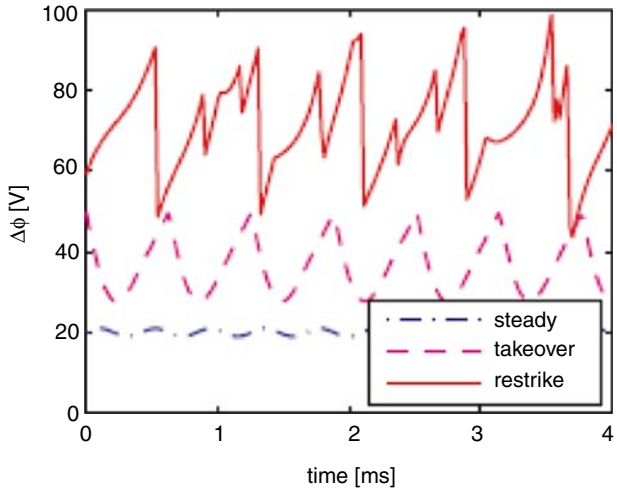

Fig. 3 The voltage as a function of time for the three main torch-running modes (Ref 1)

last two (Ref 3, 5). The main characteristics of these modes include:

- The steady mode, characteristic of a quasi-fixed arc root attachment corresponding to negligible voltage fluctuations, generally obtained with pure argon gas, and a high arc current intensity;
- The takeover mode, characterized by a quasi-periodic motion of the arc and voltage fluctuations. It can be obtained with mono-atomic gases such as pure argon or helium, provided that the arc current intensity is not too high;
- The restrike mode, characterized by a highly unstable and chaotic motion of the arc. It results from working with diatomic gas mixtures such as argon/hydrogen, nitrogen, nitrogen/hydrogen or argon/helium/hydrogen, and a medium arc current intensity.

2.2 Modeling the Plasma Generation

Several models have been proposed to simulate the plasma, and their complexities evolve with increasing computational resources. The first simulations were limited to steady plasma flows and utilized temperature and velocity profiles as input data (Ref 6-9). The average result fields of the jet flowing though the ambient atmosphere does not take into account the transient plasma flow behavior which is becoming increasingly important for suspension spraying. Two routes can be employed for a non-stationary flow outside the torch:

- A global approach, integrating the physical phenomena through the distinct equations of electromagnetic and fluid mechanics.
- A simple approach based on a Joule effect model.

2.2.1 Global Investigation of the Mechanisms Inside the Torch. The PhD thesis by Baudry opened the way for global investigations of the mechanisms inside the torch

(Ref 10-12); and subsequently, starting from the same main assumptions and numerical cases, Colombo and Ghedini (Ref 13), followed by Trelles et al. (Ref 1), improved these investigations. All these studies employed the same set of equations, based on the mass, momentum and energy conservation. This was coupled with the Maxwell equations for electromagnetism effects based on the local thermodynamic equilibrium (LTE) assumption for the gases, which supposes that all the species are at the same temperature. While Baudry (Ref 10) considered the flow in the torch as laminar, Colombo and Ghedini (Ref 13) used almost the same hypothesis and conditions, apart from the turbulence assumptions, by introducing LES formulation for calculation in the torch and downstream from it. Another difference concerns the hypothesis regarding the enforcement of the arc root.

In Ref 10, the arc root is assumed to be a high-temperature column in which the electrical field is above a critical value, which leads to an electrical short circuit. The displacement of this area results in a new column while the old one burns out. This approach has provided reasonable results for argon and argon/hydrogen operating conditions, while the values of the main parameters (frequency and arc voltage magnitude) did not fall within the correct range.

In Ref 13, there was no enforcement of the restriking of the anode in the region where the electric field intensity was sufficiently high: a uniform zero electric potential condition imposed on the anode wall was adequate. The argon arc movement seemed reasonable; however, no information was given about the arc voltage and the frequency of the restrike mode… Apparently, no multi attachment seemed to be visible, as was expected according to Ref 11. In Ref 1, an artificially high electrical conductivity was imposed near the anode. With this hypothesis, results remained similar to those of Baudry. All these investigations show that the main problem continues to be the expense of the boundary layer near the anode including the surface state of the wall in terms of electrical as well as thermal problems.

Going further, Trelles et al. (Ref 14, 15) integrated a non-local thermodynamic equilibrium (NLTE) assumption in the calculation by introducing a two-temperature model of argon plasma. A global comparison of the NLTE and LTE results with experimental data demonstrated an advantage of the NLTE model: these calculations showed an upgrading of the behavior, more particularly the voltage drop and the fluctuation frequency signals.

On their side, He-Ping Li et al. (Ref 16) used the same global model for a transferred argon arc plasma torch. Before this, time-dependent two-temperature chemical non-equilibrium modeling was studied, taking into account the chemical reactions between the various species. Tanaka (Ref 17) analyzed the inductive coupled plasma torch with such tools in the case of an argon/nitrogen plasma mixture.

2.2.2 Enthalpy Model Based on the Joule Effect. Several papers (Ref 18-21) have proposed the use of the enthalpy model, and the first description was based on a cylinder heating volume, inside the anode, in which only the Joule effect was considered. This implies knowing the average operating parameters of the torch, such as the arc current intensity, the voltage, the cooling losses… The only criterion for validating the model is the thermal efficiency rate of the torch: in a steady configuration, the length of the heating volume is adjusted to give rise to an agreement between the experimental and calculated thermal efficiency rate. Improvements have been integrated in the model (Ref 22) by introducing a rotated truncated cornet as the heating zone close to the torch exit (Fig. 4). The length, l, and the rotation angle frequency, γ, of the heating zone were then linked to the time-dependent voltage variations while the angle, β, of the truncated side depended only on the nature of the gas. This is a simple way to reproduce the constriction of the electrical arc due to the nature of the plasma gas: for a diatomic gas-argon mixture leading to a strong constriction, β is lower, while for an inert gas mixture (Ar/He), β grows due to lesser constriction. Thus, this model can provide a decent simulation of the transient flow but does not present the possibility of studying the arc behavior. The model has been used in this work and the obtained results are presented in the next section. Global information and hypotheses can be found in Ref 22.

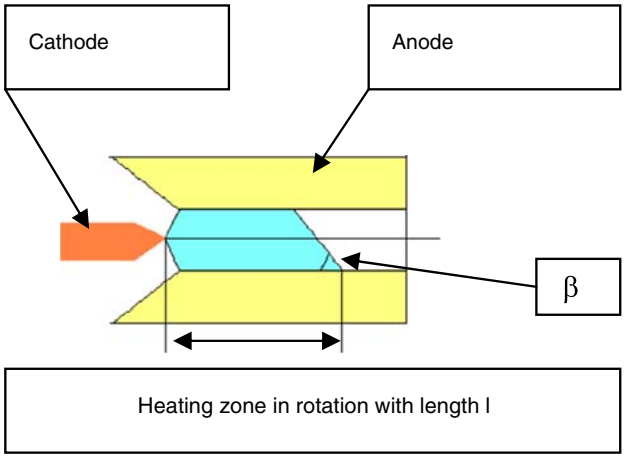

Fig. 4 A schematic of the simple model based on the Joule effect

2.3 Turbulence Model for Plasma Flow

The spreading of turbulence in the mixing layer of the plasma jet has been described by Pfender et al. (Ref 23). It governs the engulfment of the ambient atmosphere into the jet and must be accounted for through the modeling approach. Two models for plasma flow are the most common.

2.3.1 The *k*-ε Model. The *k*-ε Reynolds averaged Navier-Stokes (RANS) model is the most employed in the two-equation-model formulation. Its computational simplicity makes it an efficient tool for practical short-term industrial applications, in spite of its limitations. Generally, default constant values are used (Ref 7, 21, 22). Comparisons of various formulations of the *k*-ε model

(Ref 21) have demonstrated a too fast cooling of the plasma jet and either an underestimation (Ref 21) or a decent agreement (Ref 22) of the air engulfment. The flow inside the torch seems to be laminar before becoming turbulent downstream, but this transition is not accurately reproduced by the k-ε model (Ref 7).

2.3.2 Large Eddy Scale Simulation. Recently, studies combining a Large Eddy Simulation (LES) model with the frequently employed Smagorinsky sub-grid scale model have appeared. However, with respect to the nature of the plasma gas issued into air atmosphere, LES simulations present improvements with regard to the flow and the mixing of the plasma gas with atmosphere (Ref 24, 25). Colombo and Ghedini (Ref 13) used this model for simulating the global behavior of a torch and the downstream expansion of the argon jet into the air atmosphere. For an Ar/H_2 plasma, Balmigere compared data from the RANS and LES turbulent models (based on a steady velocity at the inlet and temperature profiles) with results from experimental measurements (Ref 26).

2.4 Plasma/Particle Interactions

For classical spraying processes, the powder is introduced into the plasma jet with the help of a carrier gas. The main purpose of this gas, generally argon due to its high density, is to allow the penetration of the powder into high-velocity and high-temperature plasma fields. The impact of the carrier gas flow on the plasma jet has been investigated by several authors (Ref 27, 28), and slow deformations of the jet (measured by deflecting angles of less than 2° for a gas flow rate of 0.339 STP m^3/h) have been pointed out (even with low carrier gas flow rates). In such cases, cooling, and to a lesser extent, slowing effects of the plasma jet, are the greatest consequences. The correct regulation of the carrier gas flow rate is thus more important: the particle momentum must be higher than that of the plasma jet, but the necessity of avoiding the cooling down of the flow fixes the limitations. Several assumptions on particles withstand the modeling approach of particle injection into the jet. The particles are assumed to be spherical without any deformations. For the heat propagation within the particle, two models (with either a homogenous temperature or a 1-D temperature gradient) can be used. Both depend on the BIOT number (Bi), which is defined as the ratio between the thermal conductivity of the boundary layer and the thermal conductivity of the particle. When Bi is less than 0.03, the particle temperature can be treated as uniform, whereas for higher Bi, the heat conduction cannot be neglected. This last case permits the juxtaposition of several phases depending on the heat flux and the cooling received by the particles (Ref 22).

Another main phenomenon concerns the so-called Knudsen effect or non-continuous effect, related to the gas mean free path (l) relative to the particle diameter (d_p). The Knudsen number, Kn, i.e., the ratio of these two parameters, expresses the discontinuous effect that cannot be neglected as soon as $Kn > 0.01$. It is introduced by a correction factor on the drag force coefficient in the momentum equation and on the Nusselt number in the energy conservation equation. The results presented in the next section take into account the Knudsen effect and the heat conduction within the particle.

2.5 Plasma/Liquid Interactions

While the injection of liquid, such as fuel in an engine, is an important field of investigation, the interaction of the liquid injected in a plasma of a classical spraying flame (such as HVOF) is a new and original field of study. As often, experimental investigations (Ref 29) have opened the door to understanding the first behavior of the liquid sheet interacting with the flame. After these observation rounds, numerical approaches are carried out. Two routes are explored. The first uses tools that are actually available and analyzes the behavior of lone and calibrated droplets (generally of water) interacting with the gas (Ref 30-32). The aerodynamic phenomena are investigated through classical break-up models, such as TAB or ETAB. In this case, only Basu and Cetegen (Ref 32) integrated the vaporization and the internal precipitation. The second route attempts to analyze the global problem from the injection of a continuous liquid jet into the plasma to its primary and then secondary break-up (Ref 33). This route implies the development of novel numerical multi-scale approaches. The main results will be presented in a later section of this paper.

3. Model, Assumptions, Equations

This section presents the CFD codes that were used in this work. Two CFD codes are introduced here, and the reasons for this are twofold. First, the study started with the FLUENT code, using the RANS turbulence model to reproduce classical plasma spraying with micrometric particles. Subsequently, extended investigations were carried out on suspension plasma spraying with the global analysis of the process. For this, a collaboration was carried out between the two teams implicated in this paper and the decision was made to work in a Euler configuration with the AQUILON code, as this would facilitate the development of new models and tools to simulate the transition from a continuous liquid jet to small droplets.

3.1 Computational Fluid Dynamic Codes

Depending on the manner of spraying, i.e., either classical plasma spraying with isolated particles or suspension injection plasma spraying leading to atomization of the liquid sheet, calculations were run with respectively the FLUENT V6.2.12 commercial package (www.fluentusers.com) or the TREFLE-home-made AQUILON codes implemented with the enthalpy model detailed in Section 2.2.2. The latter option involved the erratic truncated cornet rotating movement and the longitudinal displacement, both tuned with the arc tension fluctuation frequency.

The equations used in FLUENT have been completely detailed in (Ref 22) while those used in AQUILON are

presented in Ref 33. The numerical schemes can be found in the same papers.

3.2 Basic Assumptions

The plasma, considered as a continuous Newtonian mono-fluid, is assumed to be in the local thermodynamic equilibrium (LTE) that is optically thin and chemically inert. In the FLUENT calculations, the flow is subsonic and the compressibility effects are neglected. In the AQUILON runs, on the other hand, the compressibility is taken into account. At high temperature, provided that the LTE assumption is satisfied, the interactions between ionic and electronic species from the plasma gas are used through transport coefficients and thermodynamic properties. As no magnetic effects are considered, the input gas vortex is also neglected: these phenomena contribute significantly to the arc root displacement in opposite or combined ways. Neglecting one thus implies the same consideration for the other. This assumption has been validated in Ref 34, during an analysis with identical operating conditions, while Ref 35 demonstrated the disappearance of the swirl as soon as the plasma column was stable. The radiation losses (Ref 22 for an Ar/H_2 mixture, Ref 36 for Ar/He, Fig. 5) were introduced by using a sink term in the enthalpy equation.

3.3 Heating Model

No new developments have been conducted on the model since the publishing of the two previous papers (Ref 22, 37). The β angle changes depending on the nature of the gas in order to reproduce the causal constriction of the electrical arc. The values are detailed in the following section.

4. Calculations and Experiments

Two plasma spraying cases are here presented because of their different electrical arc fluctuation modes: one with an Ar/H_2 mixture (restrike mode), and the other with an Ar/He mixture (takeover mode). An important reason for using Ar/H_2 is the large number of investigations dedicated to this mixture with regard to classical plasma spraying. Argon/helium, on the other hand, is used more for suspension plasma spraying due to its less significant fluctuations.

4.1 Experiments

The input data (Ref 38) are summarized in Table 1. The plasma gun had a SULZER METCO design with an anode diameter of 6 mm. Figures 6 and 7 show the experimentally obtained transient arc voltage signal versus time used in the simulation. These data were directly extracted from experimental measurements while, in previous work, only fitted signals have been integrated in the simulation.

Plasma photographs were obtained by a long distance microscope (QUESTAR FR1) coupled to an intensified CCD camera (ANDOR ISTAR 720) without any filter. The optical resolution was approximately 20 μm while the time resolution was on nanosecond scale. The exposition time was 200 ns.

4.2 Calculations

4.2.1 With FLUENT CFD. The grid consisted of a mixture of hexahedrons and tetrahedrons in the center zone and involved 919,584 nodes. The flow zone, outside the torch, was 140 mm long and exhibited a continuously growing width, from 30 mm at the torch exit to 100 mm at the outlet. This configuration has been used to reduce the mesh number while decreasing the interactions of the flow

Table 1 Operating plasma conditions

Gas mixture, slm	Ar/H_2 (45-15)	Ar/He (30-30)
Average arc voltage, V	65	40
Average arc current, A	500	700
Average electric power, W	32500	28000
Thermal efficiency rate, %	50	64
Arc fluctuation frequency, μs	240	200

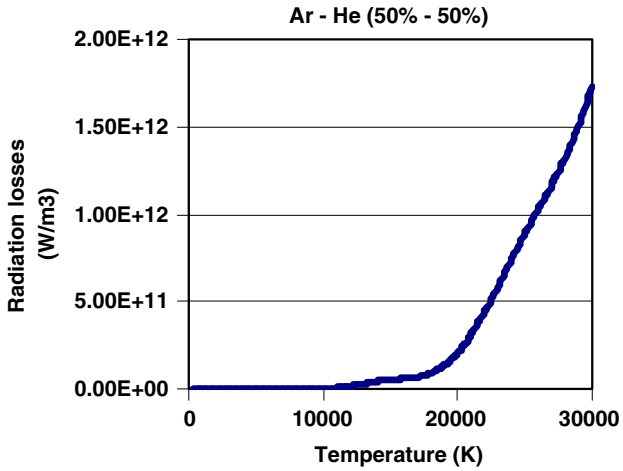

Fig. 5 Radiation losses vs. temperature for an Ar/He mixture (50 mol%-50 mol%)

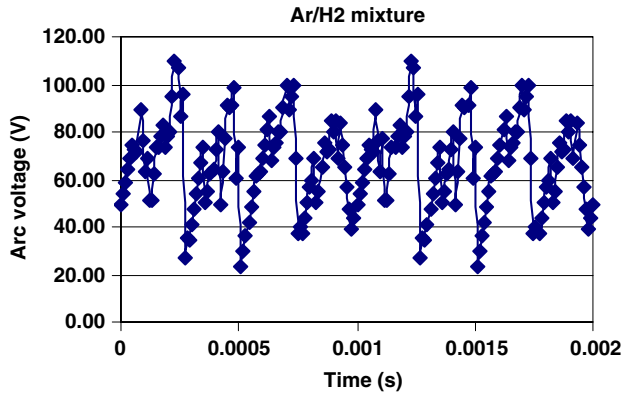

Fig. 6 The arc voltage signal vs. time as input data for the Ar/H_2 mixture

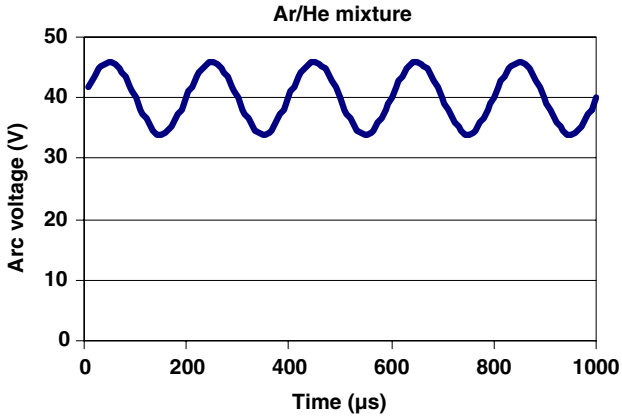

Fig. 7 The arc voltage signal vs. time as input data for the Ar/He mixture

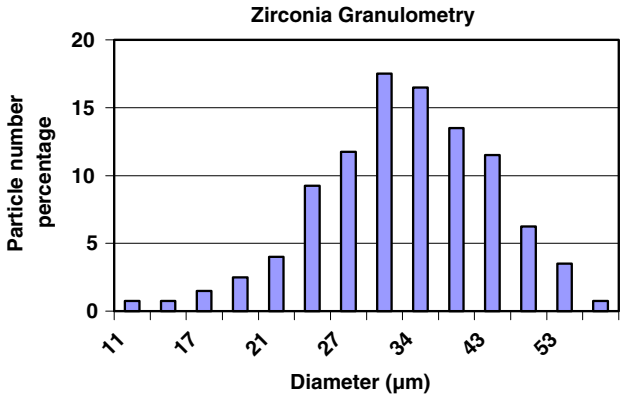

Fig. 8 The zirconia granulometry distribution

with the open boundary conditions. All other considerations are detailed in Ref 22.

For classical particle plasma spraying, the zirconia particle treatment integrates the heat propagation inside the particles as detailed in Ref 37). The granulometry distribution of the particle injected is represented in Fig. 8.

Several particles of each range (11, 19, 21, 24, 27, 30, 34, 38, 43, 48, 53, and 60 µm) were injected with an argon carrier gas (5 slm) at random positions inside an injector (1.6 mm in diameter and 20 mm in length), 6 mm from the torch exit and 9 mm from the torch axis.

4.2.2 With AQUILON CFD. In the case with only plasma flow, the calculation domain was a cube of dimension 85 mm × 100 mm × 100 mm. The calculation grid contained 486,720 cells. The mesh was refined in the central zone where the flow plasma developed, and the unsteady time step was equal to 10^{-6} s. The turbulence model was of LES type, and the plasma torch was not explicitly simulated. The temperature, concentration of Ar-H_2 (equal to 1) and velocity outlet conditions of the torch were enforced at the boundary of the calculation domain from previous FLUENT results. The boundaries were assumed to be free, and a zero velocity flux, temperature, concentration and volume fraction were imposed. All other considerations can be found in Ref 33.

For suspension plasma spraying, the calculation domain was a cube of dimension 10 mm × 10 mm × 10 mm, and the calculation grid contained 1,680,000 cells. The unsteady time step was equal to 5×10^{-8} s, and the position of the suspension injector was 3.3 mm downstream from the torch exit and 5 mm from the gun axis. Its hole diameter was 150 µm. Here, the liquid was pure water, without any nanoparticles, introduced with a direct 40 m/s velocity (which corresponds to a 0.8 MPa injection pressure). No fluctuations at the boundary of the liquid sheet were imposed. In this case, only aerodynamic effects were taken into account. In the first instance, the thermal effects of the plasma on the liquid with regard to phase change and vaporization were not integrated.

5. Results and Discussion

The following section provides a comparison of the simulation results with experimental measurements for the various gas mixtures with regard to the plasma generation.

5.1 Plasma Generation

Figures 9-12 present the behavior of the downstream flow outside the torch, with respectively an argon/hydrogen mixture and an argon/helium one at various moments. All the calculations of the next two paragraphs were obtained with FLUENT and the RANS turbulence model.

5.1.1 Argon/Hydrogen. As previously explained, numerous papers have been devoted to the analysis of argon/hydrogen plasma gas behavior, and the simple heating model has thus been validated by comparing results from simulation and experiment (Ref 22, 33, 37). This model describes, through the imposed dissymmetry, the behavior of the jet due to the arc attachment. The following figures show the displacement of the temperature zones (around 13000 K) 6 mm downstream the torch exit (the scale remains the same for all the pictures and the white zone corresponds to 300 K).

While the flow is quite laminar at this distance from the gun exit, some excrescences of gas puffs can be seen at several points (to the lower left in the first picture, and at the bottom of the two others).

In a next step, comparisons of longitudinal flow are proposed in Fig. 10 where the temperature-simulated and photographed behaviors of the plasma jet are shown. In this figure, puffs of hot gas were given off when the length of the electric arc was shortened. The expansion of the gas closer to the anode exit could, after studying the global simulation images, be explained according to the following. The attachment of the arc root was inside the anode for all cases, but more or less close to the exit. Arriving at its maximal length, the arc rapidly became shortened,

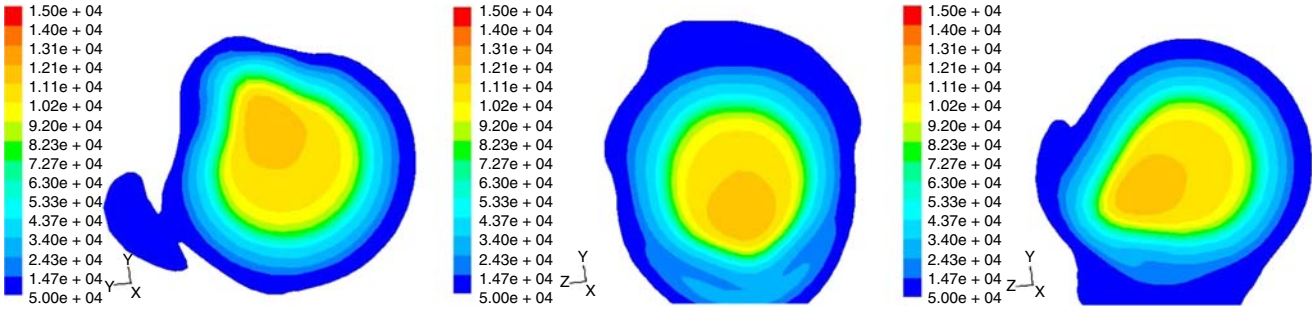

Fig. 9 Cross sections of the calculated Ar/H_2 plasma jet temperature 6 mm downstream from the torch exit and at three times: 4.83 ms (left), 5.017 ms (middle), and 5.795 ms (right)

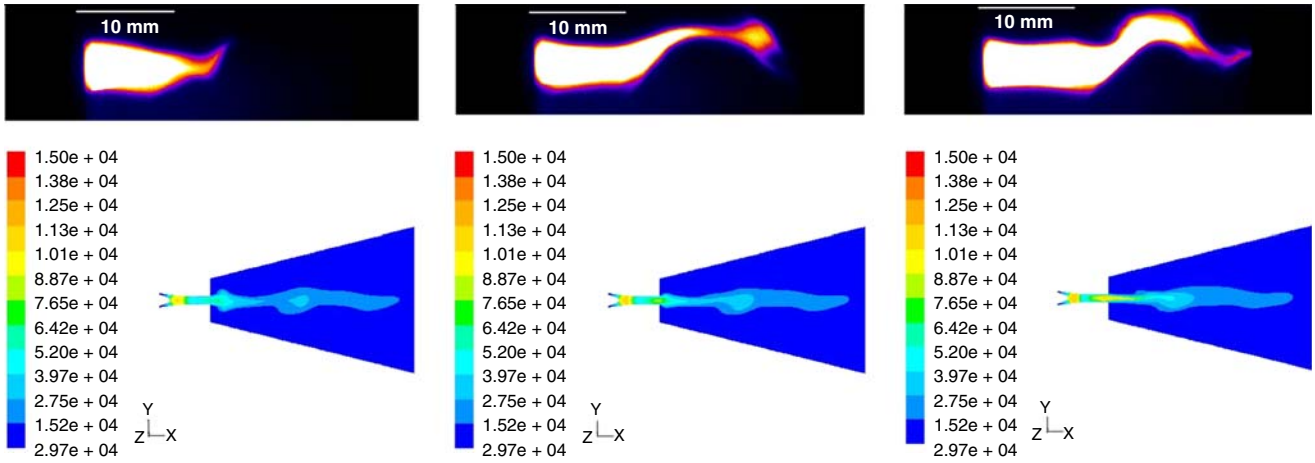

Fig. 10 Comparisons between experiments and simulations with the RANS turbulence model for the temperature of an Ar/H_2 flow at various instants

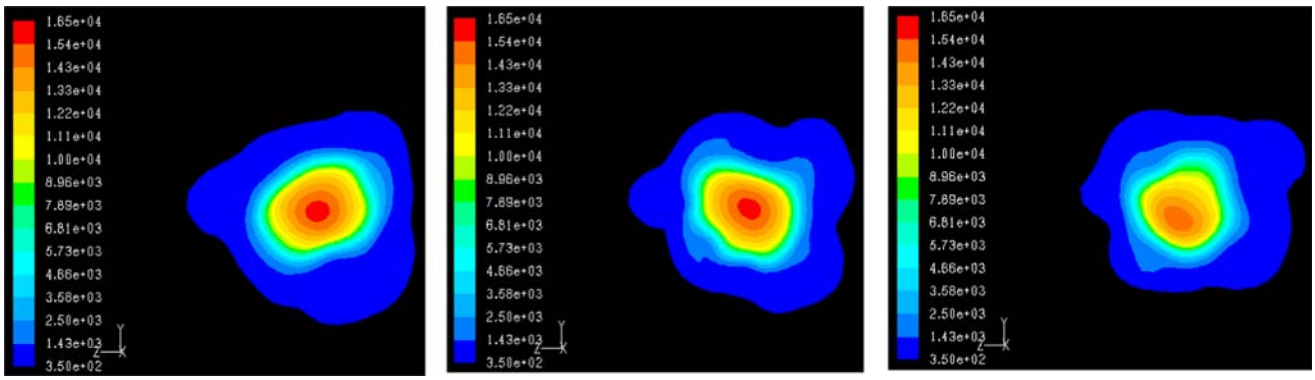

Fig. 11 Cross sections of the calculated Ar/He plasma jet temperature 6 mm downstream from the torch exit and at three times: 64 ms (left), 69 ms (middle), and 79 ms (right)

leaving an unattached hot gas volume while the hot column was upstream. Due to the aerodynamic forces, this volume moved to the anode exit, cooled down and decelerated while the column behind it grew, pushing it away. When the gas volume exited the anode, it went through a rapid expansion. This phenomenon was only visible in the restrike mode due to the constriction of the arc column and the electrical arc jumps. Moreover, it could not be observed under operating conditions of argon/helium plasmas due to the continuous arc root motion without jump. It was quite difficult to reproduce the dispersion of the jet with the k-ε turbulence model since it fit the instability too much. This point will be further discussed in Section 5.2.

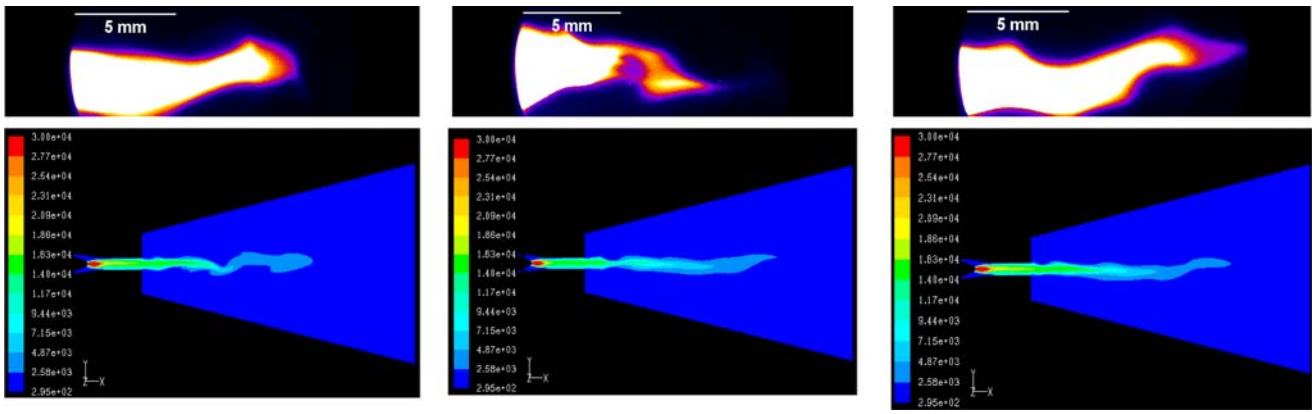

Fig. 12 Comparisons between experiments and simulations for the temperature of the Ar/He flow at various instants

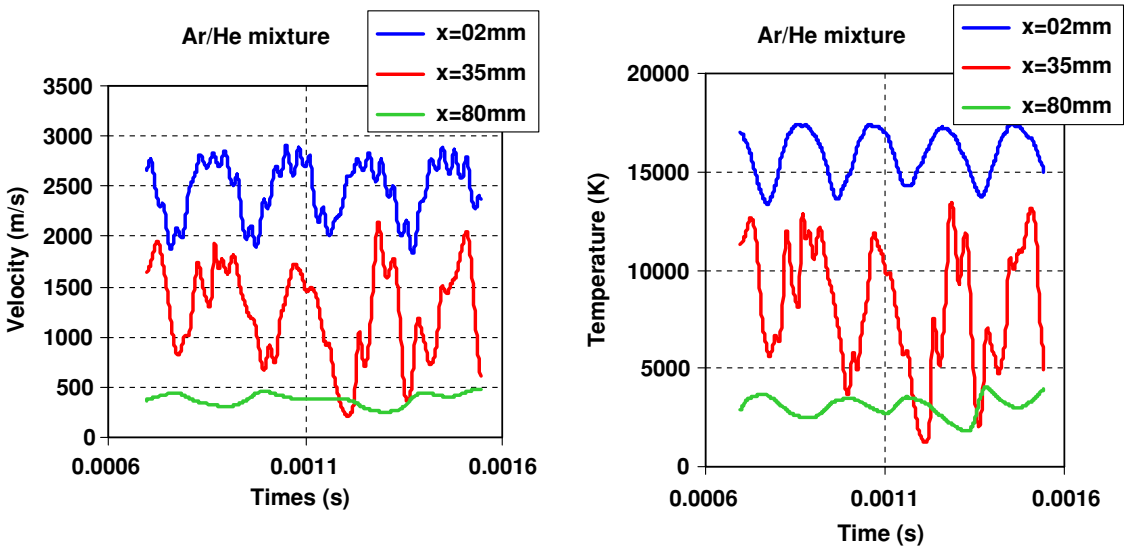

Fig. 13 The center-line velocity (left) and temperature (right) of the Ar/He jet vs. time at three points downstream from the torch exit 2, 35, 80 mm from top to bottom

5.1.2 Argon/Helium. This section presents the first simulation results concerning the argon/helium plasma gas mixture. After investigations, only experimental results concerning Ar/He temperature measurements (Ref 39) were found in the literature apart from its behavior, as described in Ref 3-5.

We here see the displacements of the temperature zones at the position 6 mm downstream the torch exit (the scale remains the same for all the pictures and the black zone corresponds to 300 K). Similar observations can be obtained when analyzing the jet velocity. Due to the sinusoidal arc voltage signal and the less important constriction of the jet, the highest temperature zone (with a maximum of around 16500 K) remained more or less centered while the jet maintained its almost circular shape, without displaying any significant deformation. The difference can be seen in Fig. 9 for Ar/H_2).

In this configuration, the fluctuation of the jet in the transversal direction was less present in the photographs and the simulation images (Fig. 12). The flow ran straight with a low deviation amplitude and could be well reproduced by the simulation. Figure 13 shows the center-line velocity (left) and temperature (right) of the jet at various stand-off distances downstream the gun exit. In the temperature curve, the average center-line measurements (Ref 39) have been added at the two first measurements points (bold lines noted respectively $P = 2$ mm and $P = 35$ mm). At $x = 2$ mm, the low fluctuations on the sinusoidal curve were due to the random 360° displacement of the electrical arc on the anode wall. At this distance, the jet was still laminar. For the next stand-off point, the turbulence and the air engulfment caused the center-line velocity and temperature to become highly fluctuating. At a large distance, the fluctuations decreased.

The average center-line temperature reached respectively 15000 and 8100 K at $x = 2$ mm and $x = 35$ mm (Ref 39), and the calculated temperature fluctuated around these values. Thus, despite a too high local temperature

(30000 K) near the cathode tip, the temperature downstream seemed realistic when compared to the experiments. This was logical due to the agreement between the experimentally obtained and simulated thermal efficiency rate of the torch, used as validation criteria.

5.2 Analysis of the Flow

One objective was to analyze the influences of the fluctuating electrical arc movement and of the turbulence model upon the downstream flow. In order to do so, the argon/hydrogen stationary case was simulated with both the RANS turbulence model, and the LES turbulence model.

In Fig. 14, without any arc root displacement in the anode, the development of instabilities could be clearly observed through the mixing of the environment air with the jet only for the LES turbulence model simulation and thus not for the RANS model simulation. In Fig. 15 can be seen the instability development (compared with experiments) with LES model while no arc moving. This led to the conclusion that, when using the RANS model, the aforementioned fluctuations were completely due to the electric arc motion, thus demonstrating:

- the superiority of the LES approach for simulating jet dynamics and
- the necessity of taking into account the electrical arc movement to obtain a significant dispersion of the hot gas plume, as seen in Fig. 14.

An upgrading of the computational tools would render this possible. For simulations (in progress) with an Ar/He mixture used in suspension plasma spraying, the LES turbulence model will be privileged.

5.3 Particle Plasma Spraying

This section presents comparisons of experimental (Ref 40) and calculated velocities and temperatures of

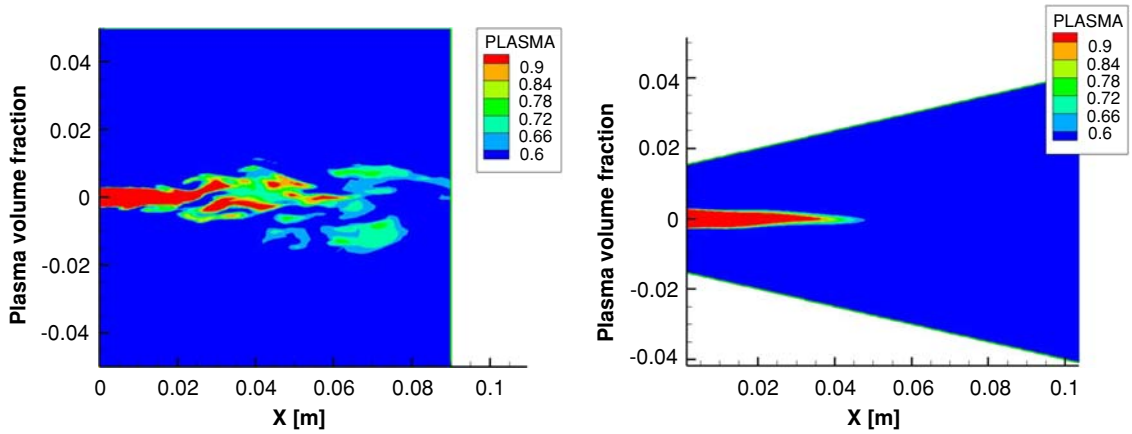

Fig. 14 A comparison of the Ar/H_2 stationary plasma flow with the LES turbulence model (left) and the k-ε model (right)

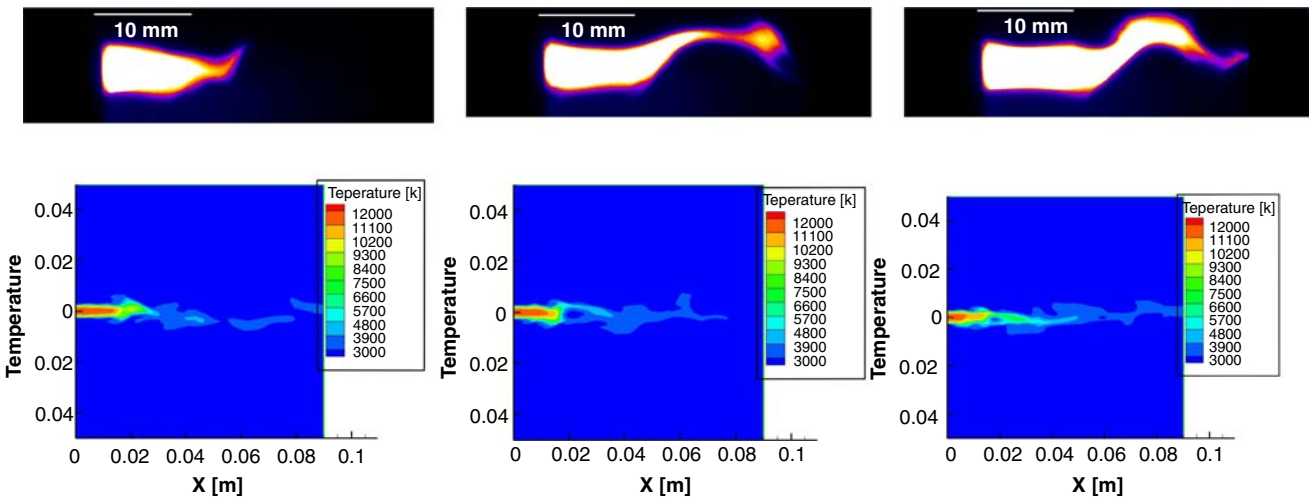

Fig. 15 Comparisons between experiments and simulations obtained with the LES turbulence model for the temperature of the Ar/H_2 flow at various instants

different sized particles depending on the Y transversal deviation at a 120-mm stand off distance from the plasma torch exit (Fig. 16). The experimental measurements were obtained with a DPV 2000 diagnostic tool (Ref 40). Particles with diameters of less than 19 μm were completely vaporized and never reached the substrate. For the velocity, the trend was correctly reproduced despite an underestimation of the deviation concerning the largest particles. For the temperature, however, the agreement was not very good. In this case, the results for the lightest particles deviated from their experimental counterparts while the data concerning the large particles corresponded to the correct values.

In fact, no convincing assumption with regard to the poor thermal treatment of the lightest particles could be put forward. The only plausible reason involved their limited penetration into the plasma plume high-temperature fields. However, as these hot zones are the same as the high velocity ones, the agreement for the velocity should also be bad—which it was not. Due to their low mass inertia, one could imagine that the particles were sensitive to random gas movements and later became trapped by the flow, after the high-temperature fields. However, if they remained in the hot flow, they completely disappeared by vaporization (Ref 41).

5.4 Suspension Plasma Spraying

For all the following figures, the gas, originating from the torch, entered on the middle-left and the flow was directed to the right. Figure 17 presents preliminary results consisting in the Ar/H_2 plasma concentration field in two slices perpendicular to the water jet and the isosurface of the $C = 0.5$ water concentration. The calculation end time was 5×10^{-5} s.

After penetration of the liquid into the plasma jet, a distortion of the sheet rapidly took place: the liquid jet twisted and fluctuations grew on its surface. Its atomization occurred a few mm later. In this case, the thermal effects were not included, and this atomization was consequently incomplete. Nevertheless, the appearance of large droplets can be observed. The effect of the instability due to turbulence can be shown in a horizontal cross section with the separation of the sheet in two independent

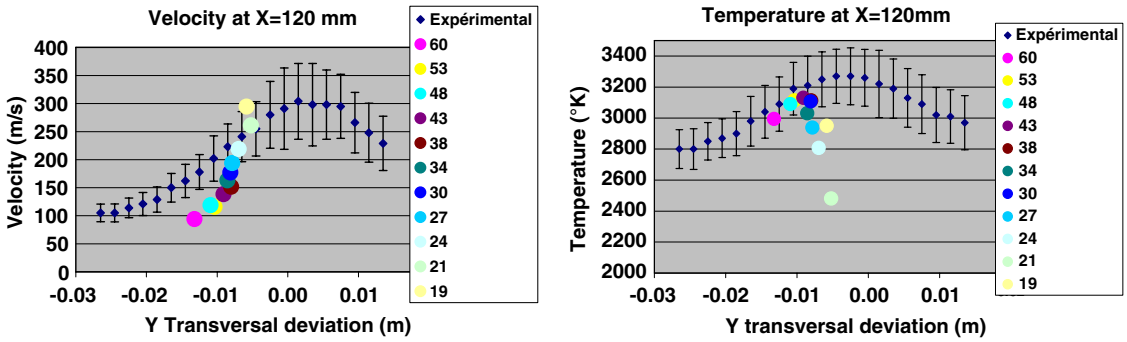

Fig. 16 Comparisons between experiments and simulations for the velocity and temperature of zirconia particles 120 mm from the torch exit vs. the Y transversal deviation

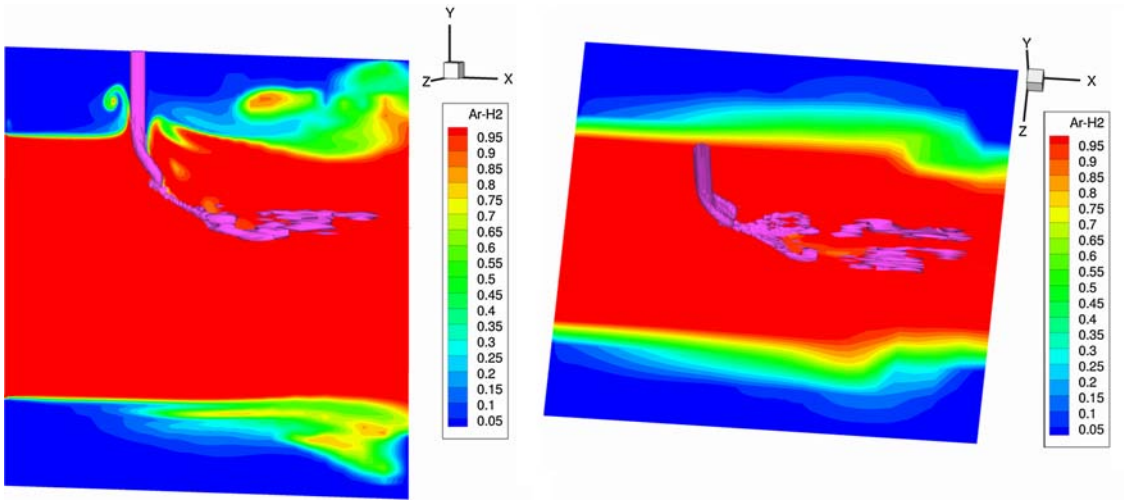

Fig. 17 Vertical (left) and horizontal (right) cross sections of an Ar/H_2 and $C = 0.5$ liquid jet concentration reaching the torch axis

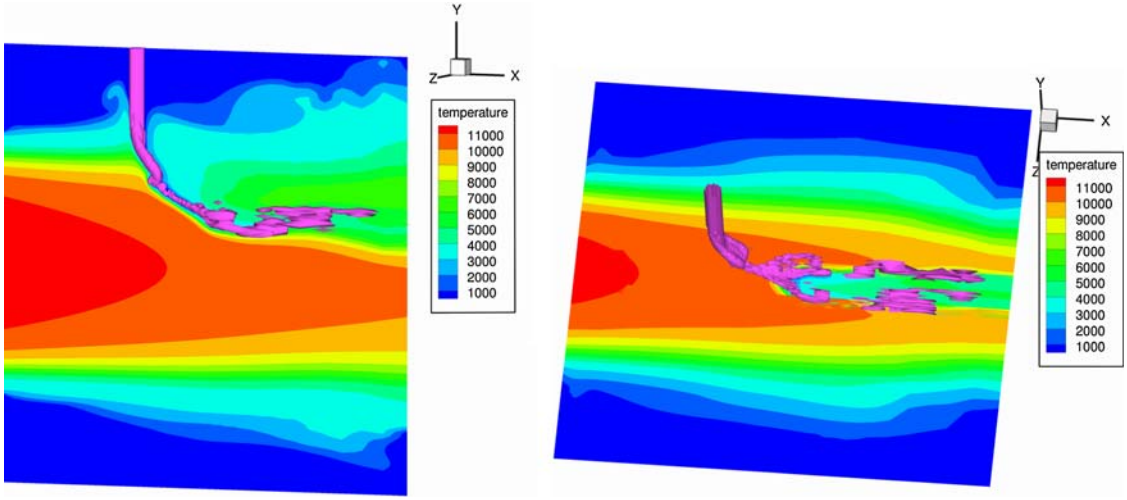

Fig. 18 Vertical (left) and horizontal (right) cross sections of an Ar/H_2 temperature and liquid jet $C = 0.5$ concentrations reaching the torch axis

groups of droplets whereas it is not visible in the vertical cross section. No air penetration could be noticed since the Ar/H_2 concentration was maintained as 1 in the center of the plasma jet while swirls appeared further at the jet boundary (particularly more visible on the vertical cross section).

Figure 18 presents the influence of the introduction of the liquid sheet on the temperature plasma jet. The deformation of the temperature field was well identified with a drop from nearly 11000 K to around 4000 or 5000 K. The temperature was largely overestimated as a result of neglecting the thermal effect and the fact that the water changed phase: in reality, the temperature might continue to drop. The integration of these effects is still in progress.

6. Conclusion

This paper presents numerical investigations concerning plasma spraying—from the generation of the plasma jet, using a 3-D transient ''heating zone'' model inside the torch, to the interactions of, on the one hand, a time-dependent jet with zirconia particles for classical plasma spraying, and, on the other hand, with a liquid jet and for suspension plasma spraying. The analysis was carried out by way of two turbulence models: RANS and LES. Several comparisons with experiments were presented for Ar/H_2 and Ar/He plasma flows, involving zirconia particles and a thermodynamic state at impact.

The analysis of the unsteady flow revealed that the simple ''heating zone'' model (using only the Joule effect connected with the arc voltage time-dependent signal) coupled with the LES turbulence model could relatively well reproduce the behavior of the jet, including the air engulfment. Due to the long calculation time required for the LES model, the RANS turbulence model represented an alternative with a lowest restitution in cases where one does not have access to powerful computational tools.

For classical plasma spraying with zirconia particles, the trend with regard to the velocity of particles of a large size range was similar to that of the experimental measurements versus the Y transversal deviation. However, there is still incomprehension as to why there was a poor temperature restitution for the lightest particles while the results for the biggest particles were in agreement with the experimental data.

For suspension plasma spraying, a global analysis was performed on the injection of a liquid jet in the transient plasma jet. The effects of the LES turbulence model were clearly visible with local phenomena of liquid breaking. The first results showed the deformation of both jets: the liquid displayed a primary fragmentation into large drops, and the plasma exhibited a significant drop in temperature while the thermal effect in terms of phase change on the water were not yet integrated in the model. Such an integration is under way. These encouraging results engage other new developments. For the moment, no quantitative analysis has been started, but the next step will consist in calculating certain important atomization parameters such as the mean droplet parameter. This validation is in progress through the testing of the fragmentation of a single droplet by supersonic air crossflow.

References

1. J.P. Trelles, E. Pfender, and J. Heberlein, Multi Scale Element Modeling of Arc Dynamics in a D.C. Plasma Torch, *Plasma Chem. Plasma Process.*, 2006, **26**, p 557-575
2. X. Sun and J. Heberlein, Fluid Dynamic Effects on Plasma Torch Anode Erosion, *J. Therm. Spray Technol.*, 2005, **14**(1), p 39-44
3. S. Janisson, A. Vardelle, J.F. Coudert, P. Fauchais, and E. Meillot, Analysis of the Stability of DC Plasma Gun Operating with Ar–He–H_2 Gas Mixtures, *Ann. NY Acad. Sci.*, 1999, **891**, p 407-416

4. S.A. Wurtzke, E. Pfender, and E.R.G. Eckert, Study of Electric Arc Behaviour with Superimposed Flow, *AIAA J.*, 1967, **5**, p 707-714
5. Z. Duan and J. Heberlein, Arc Instabilities in a Plasma Spray Torch, *J. Therm. Spray Technol.*, 2002, **11**(1), p 44-57
6. R.L. Williamson, J.R. Fincke, and C.H. Chang, A Computational Examination of the Sources of Statistical Variances in Particle Parameters During Thermal Plasma Spraying, *Plasma Chem. Plasma Process.*, 2000, **20**(3), p 299-324
7. C. Kai, X. Chen, and W.X. Pan, Comparison of Laminar and Turbulent Thermal Plasma Jet Characteristics. A Modeling Study, *Plasma Chem. Plasma Process.*, 2006, **26**, p 211-235
8. R.L. Williamson, J.R. Fincke, D.M. Crawford, S.C. Snyder, W.D. Swank, and D.C. Haggard, Entrainment in High-Velocity, High-Temperature Plasma Jets Part II: Computational Results and Comparison to Experiment, *Int. J. Heat Mass Transf.*, 2003, **46**, p 4215-4228
9. J.R. Fincke, D.M. Crawford, S.C. Snyder, W.D. Swank, and D.C. Haggard, Entrainment in High-Velocity, High-Temperature Plasma Jets. Part I: Experimental Results, *Int. J. Heat Mass Transf.*, 2003, **46**, p 4201-4213
10. C. Baudry, A. Vardelle, and G. Mariaux, Numerical Modelling of a D.C. Non-Transferred Plasma Torch: Movement of the Arc Anode Attachment and Resulting Anode Erosion, *High Temp. Mater. Process.*, 2005, **9**, p 1-15
11. C. Baudry, A. Vardelle, A. Mariaux, C. Delalondre, and E. Meillot. Three-Dimensional and Time-Dependent Model of the Dynamic Behaviour of the Arc in a Plasma Spray Torch, *Proceedings of the International Thermal Spray Conference*, 2004
12. C. Baudry, ''Contribution à la modélisation instationnaire et tridimensionnelle du comportement dynamique de l'arc dans une torche de projection plasma,'' Ph.D. Thesis, Limoges University, 2003 (in French)
13. V. Colombo and E. Ghedini, Time-Dependent Torch: Anode Attachment and Downstream Region Effects, *Proceedings of 17th International Symposium on Plasma Chemistry*, Toronto, Canada, 2005
14. J.P. Trelles, J. Heberlein, and E. Pfender, Non-Equilibrium Modelling of Arc Plasma Torches, *J. Phys. D: Appl. Phys.*, 2007, **40**, p 5937-5952
15. J.P. Trelles, E. Pfender, and J. Heberlein, Thermal Nonequilibrium Simulation of an Arc Plasma Jet, *IEEE Trans. Plasma Sci.*, 2008, **36**(4), p 1026-1027
16. J.P. He-Ping Li, J. Heberlein, and E. Pfender, Three-Dimensional Nonequilibrium Effects in a High-Intensity Blown Arc, *IEEE Trans. Plasma Sci.*, 2005, **33**(2), p 402-403
17. Y. Tanaka, Time-Dependent Two-Temperature Chemically Non-Equilibrium Modelling of High-Power Ar-N_2 Pulse-Modulated Inductively Coupled Plasmas at Atmospheric Pressure, *J. Phys. D: Appl. Phys.*, 2006, **39**, p 307-319
18. P. Eichert, ''Etude de l'écoulement gazeux au sein et à l'extérieur d'une torche de projection à plasma d'arc soufflé à l'aide du code PHOENIX,'' Ph.D. Thesis, Université de Franche Comté, 9 Décembre 1996 (in French)
19. P. Eichert, M. Imbert, and C. Coddet, Numerical Study of an Ar/H_2 Gas Mixture Flowing Inside and Outside a DC Plasma Torch, *J. Therm. Spray Technol.*, 1998, **7**(4), p 504-512
20. K. Remesh, S.C.M. Yu, H.W. Ng, and C.C. Berndt, Computational Study and Experimental Comparison of the In-Flight Particle Behaviour for an External Injection Plasma Spray Process, *J. Therm. Spray Technol.*, 2003, **12**(4), p 508-522
21. G. Mariaux and A. Vardelle, 3-D Time-Dependent Modelling of the Plasma Spray Process. Part 1: Flow Modelling, *Int. J. Therm. Sci.*, 2005, **44**, p 357-366
22. E. Meillot, D. Guenadou, and C. Bourgeois, Three-Dimension and Transient D.C. Plasma Flow Modeling, *Plasma Chem. Plasma Process.*, 2008, **28**(1), p 69- 84
23. E. Pfender, W.L.T. Chen, and R. Spores, A New Look at the Thermal and Gas Dynamic Characteristics of a Plasma Jet, *Proceedings of the 3rd National Thermal Spray Conference, Thermal Spray Research and Applications*, T.F. Bernecki, Ed., May 20-25, 1990 (Long Beach, CA), ASM International, 1991
24. H. Zhang, S. Hu, G. Wang, and J. Zhu, Modeling and Simulation of Plasma Jet by Lattice Bolzmann Method, *Appl. Math. Mod.*, 2007, **31**, p 1124-1132
25. E. Pfender and C.H. Chang, Plasma Spray Jets and Plasma-Particulate Interaction: Modeling and Experiments, *Proceedings of the 15th International Thermal Spray Conference, Thermal Spray: Meeting the Challenges of the 21st Century*, C. Coddet, Ed., May 25-29, 1998 (Nice, France), ASM International, 1998, p 315-325
26. G. Balmigere, E. Meillot, S. Vincent, and J.P. Caltagirone, Unsteady 3D Large Eddy Simulation of an Ar-H_2 Plasma Jet: Analysis of Initial Results, Global Coating Solutions, *Proceedings of the 2007 International Thermal Spray Conference*, B.R. Marple, M.M. Hyland, Y.C. Lau, C.L. Li, R.S. Lima, and G. Montavon, Ed., May 14-16 (Beijing, China), ASM International, 2007
27. H.B. Xiong, L.L. Zheng, S. Sampath, R.L. Williamson, and J.R. Fiwcke, Three Dimensional Simulation of Plasma Spray: Effects of Carrier Gas Flow and Particle Injection on Plasma Jet and Entrained Particle Behaviour, *Int. J. Heat Mass Transf.*, 2004, **47**, p 5189-5200
28. H.P. Li and E. Pfender, Three Dimensional 3D Simulation of a DC Transferred Arc Plasma Modeling of the Plasma Spray Process, *J. Therm. Spray Technol.*, 2007, **16**(2), p 245-260
29. K. Wittmann-Teneze, ''Etude de l'élaboration de couches minces par projection plasma,'' Ph.D. Thesis, Université de Limoges, 2001, no. 60-2001 (in French)
30. C. Marchand, C. Chazelas, G. Mariaux, and A. Vardelle, Liquid Precursor Plasma Spraying: Modeling the Interactions Between the Transient Plasma Jet and the Droplets, *J. Therm. Spray Technol.*, 2007, **16**(5-6), p 705-712
31. C. Marchand, A. Vardelle, G. Mariaux, and P. Lefort, Modelling of the Plasma Spray Process with Liquid Feedstock Injection, *Surf. Coating Technol.*, 2008, **202**, p 4458-4464
32. S. Basu and B.M. Cetegen, Modeling of Liquid Ceramic Precursor Droplets in a High Velocity Oxy-Fuel Flame Jet, *Acta Mater.*, 2008, **56**, p 2750-2759
33. S. Vincent, G. Balmigere, C. Caruyer, E. Meillot, and J.P. Caltagirone, Contribution to the Modeling of the Interaction Between a Plasma Flow and a Liquid Jet, *Surf. Coat. Technol.*, 2008. doi:10.1016/j.surfcoat.2008.11.009
34. R. Westhoff, A.H. Dilawari, and J. Szekely, A Mathematical Representation of Transport Phenomena Inside a Plasma Torch, *Mater. Res. Soc. Symp. Proc.*, Vol. 190, 1991, Materials Research Society
35. R. Spores and E. Pfender, Flow Structure of a Turbulent Thermal Plasma Jet, *Surf. Coat. Technol.*, 1989, **37**(3), p 251-432
36. M.E. Rouffet, ''Nouvelle méthode de diagnostic optique des plasmas thermiques: application au mélange Argon/Hydrogène/Helium,'' Ph.D. Thesis, Université de TOULOUSE III, 22 Septembre 2008 (in French)
37. E. Meillot and G. Balmigere, Plasma Spraying Modeling: Particle Injection in a Time-Fluctuating Plasma Jet, *Surf. Coat. Technol.*, 2008, **202**, p 4465-4469
38. R. Etchart-Salas, V. Rat, J.F. Coudert, P. Fauchais, N. Caron, K. Wittmann, and S. Alexandre, Influence of Plasma Instabilities in Ceramic Suspension Plasma Spraying, *J. Therm. Spray Technol.*, 2007, **16**(5-6), p 857-865
39. W.L.T. Chen, J. Heberlein, and E. Pfender, Diagnostic of a Thermal Plasma Jet by Optical Emission Spectroscopy and Enthalpy Probe Measurements, *Plasma Chem. Plasma Process.*, 1994, **14**(3), p 317-332
40. V. Debout, A. Vardelle, P. Abelard, P. Fauchais, E. Meillot, E. Bruneton, F. Enguehard, and S. Schelz, Investigation of In-Flight Particle Characteristics and Micro Structural Effects on Optical Properties of YSZ Plasma-Sprayed Coatings, *Proceedings of HTPP 9*, P. Fauchais and J. Amouroux, Ed. (St. Petersburg, Russia), *J. High Temp. Mater. Process.*, May 2006
41. E. Meillot, D. Guenadou, and C. Bourgeois, Effect of Time-Dependent D.C. Plasma Flow on Particle Treatment, *Proceedings of HTPP 9*, P. Fauchais and J. Amouroux, Ed. (St. Petersburg, Russia), *J. High Temp. Mater. Process.*, May 2006